



Nanosecond pulse laser scribing using Bessel beam for single shot removal of transparent conductive oxide thin film



Byunggi Kim^{a,*}, Ryoichi Iida^a, Duc Hong Doan^{b,*}, Kazuyoshi Fushinobu^a

^a Department of Mechanical and Control Engineering, Tokyo Institute of Technology, Mail Box 16-3, Ookayama 2-12-1, Meguro-ku 152-8552, Japan

^b Advanced Materials and Structures Laboratory, University of Engineering and Technology, Vietnam National University, Hanoi, 144 Xuan Thuy, Cau Giay, Hanoi, Viet Nam

ARTICLE INFO

Article history:

Received 21 June 2016

Received in revised form 21 November 2016

Accepted 23 November 2016

Keywords:

Nanosecond laser scribing

Pulsed laser ablation

Transparent conductive oxide thin film

Bessel beam

Self-reconstruction

ABSTRACT

Nanosecond laser Bessel beam scribing on the TCO thin film was investigated to improve processing precision and robustness of optical system. Fundamental wave (1064 nm) of Nd:YAG laser was shaped into high-quality Bessel beam by using novel optical system consisting of axicons and convex lens. Spatial FWHM of the beam was only 1.5 μm in the present context, and significantly precise scribing with minimum width of 2.3 μm was achieved on 600–700 nm-thick FTO film with electrical isolation. Furthermore, due to the critically deep focal length of millimeters-order, robustness on sample positioning was greatly improved. Additionally, experimental results showed that single shot removal of entire film can be achieved using film side irradiation unlike conventional Gaussian beam. Temperature distribution during the process was calculated by a numerical model in which we have taken into account beam propagation inside the film to give comparison with a Gaussian beam irradiation. The calculation results showed that only Bessel beam is self-reconstructed behind plasma shielding so that entire film can be removed by single shot. Our findings suggest that Bessel beam can be used for efficient IR scribing with significantly high quality without selecting substrate material.

© 2016 Elsevier Ltd. All rights reserved.

1. Introduction

Recent spread of opto-electronic devices in various industrial field has boosted increasing use of transparent conductive oxide (TCO) thin films such as indium tin oxide (ITO), zinc oxide (ZnO), and fluorine doped tin oxide (FTO). Its one of the most representative applications is thin film photovoltaics (TFPV). Because of large size of TFPV, nanosecond pulse laser scribing, which can be implemented easily with significantly low cost and fast fabrication speed, has been used widely for patterning process of thin film layers [1–5]. However, scribing width less than several tens of micrometers cannot be obtained by traditional Gaussian beam irradiation. As scribed area of TFPV devices cannot generate electricity with sunlight irradiation, narrow scribing is a key technology to high energy conversion efficiency. In 2014, few micrometers wide femtosecond laser scribing was reported by Krause et al. [6]. Their findings showed that real cold ablation of fs laser, which is governed by interaction between material's electrons and laser, will lead to remarkable progress in thin film scribing industry. However, implementation of fs laser still require too

large cost compared to ns laser. Therefore, we have focused on improving ns laser processing by controlling optical parameters such as spatial profile of the beam [7–9].

In general, it is known that optically thick film is removed with substrate side irradiation which leads to stress-assisted ablation induced by steep temperature gradient at film/substrate or film/film interface [1,10,11]. On the other hand, we experimentally demonstrated that under near-IR laser irradiation optically thin film such as the TCO is removed thermally from its surface in our previous study [12]. Irrespective to irradiation direction, surface temperature of the TCO film increases considerably because of heat conduction to the substrate. For ns laser processing, as plasma shielding accompanied by thermal ablation at the TCO thin film surface interrupts absorption of laser beam, substrate side irradiation has great advantage on complete film removal process with single shot. However, use of substrate side irradiation is limited to the cases that substrate material is rigid and transparent. As plasma shielding is less significant with short wavelength [13], film side irradiation of ultraviolet laser can be used in the case that film thickness is several tens of nanometer. However, film removal process using UV laser is strongly dependent on film thickness and sensitive to substrate damage.

In the present study, we report experimental achievements of Bessel beam scribing of TCO thin film, taking advantage of narrow

* Corresponding authors.

E-mail addresses: kim.b.aa@m.titech.ac.jp (B. Kim), doan.d.aa.eng@gmail.com (D. H. Doan).

beam width and deep focal depth to improve precision of scribing and robustness of optical system. In addition, propagation of Bessel beam wavefront generated by axicon was of interest, reconstruction of beam intensity behind obstacle [14] is expected to help avoiding plasma shielding to some extent. Experimental data was analyzed numerically with the thermodynamic model with consideration of beam propagation inside the film. The experimental and theoretical investigations in this article will demonstrate advantages of Bessel beam in the TCO thin film scribing process.

2. Experimental setup

Fig. 1 shows schematic illustration of experimental setup. The near-IR wavelength of 1064 nm was used from Nd:YAG laser with pulse width of 5.5 ns (FWHM). Original spatial beam profile was nearly top-hat. In order to increase quality of the Bessel beam, the original beam was expanded and shaped into perfect circle by being passed into circular aperture. Plane wavefront can be obtained by this manipulation. Demagnifying telescope consisting of axicon-convex-convex lenses (in order) is generally used to obtain narrow quasi Bessel beam [15–17]. In the present context, we replaced second convex lens with another axicon. Bessel beam generated by this method has slightly spherical wavefront so that beam width changes on the optical direction. Nevertheless, this transform is more advantageous with the extremely longer focal depth and easier optical adjustment free from using two convex lenses. Hence, we adapted this combination considering robustness of the optical system. For the Gaussian beam irradiance, conventional convex lens focusing with $f = 100$ mm was used instead of Bessel beam shaper.

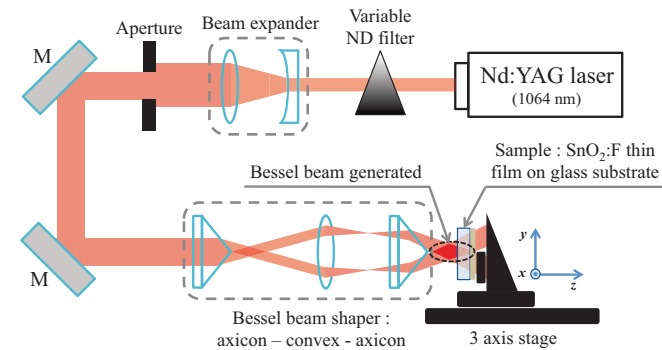


Fig. 1. Schematic illustration of experimental apparatus. A modified demagnifying telescope consisting of two axicons and a convex lens was used to shape narrow Bessel beam with crucially deep focal depth.

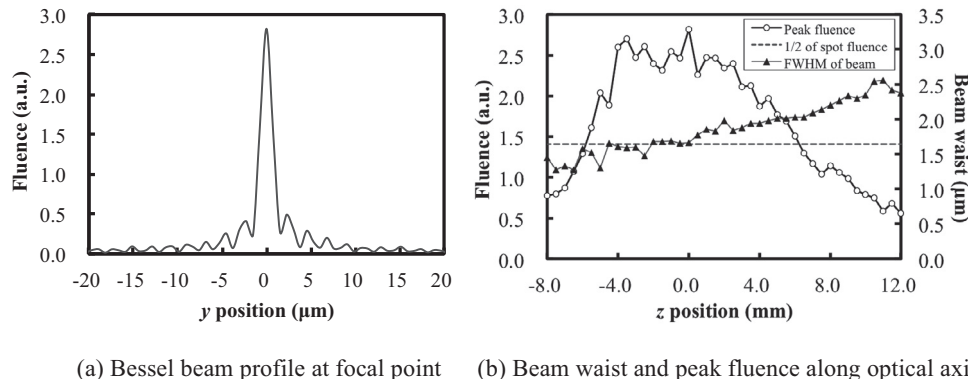


Fig. 2. Spatial profiles of the Bessel beam in the present context. Spatial FWHM and focal depth of the beam were measured as 1.3–2.0 μm and 11.5 mm respectively.

Table 1
Experimental conditions.

Parameter	Unit	Value
Wavelength, λ	nm	1064
Pulse width, t_p	ns	5.5
Focal length, f	mm	100
Bessel beam FWHM	μm	1.3–2.0
Gaussian beam waist	μm	24
FTO thickness, h	nm	600–700
Substrate thickness	mm	1.8

Fig. 2 indicates Bessel beam profile and change of beam waist and peak fluence along the optical axis. Spot with the largest peak fluence was determined as a focal spot. As experimentally obtained Bessel beam has imperfect separation between 0th order peak and 1st order lobe, we used FWHM instead of 13.5% width for Bessel beam. FWHM of generated Bessel beam was 1.3–2.0 μm , and focal depth (determined based on the area with fluence larger than half of the peak fluence) was measured as 11.5 mm. On the other hand, beam waist and focal depth of the Gaussian beam in this study were 24 μm and 1 mm. Therefore, Bessel beam had crucial advantages with extremely narrow beam width and deep focal depth compared to conventionally focused Gaussian beam.

The FTO thin film with 600–700 nm thickness on the glass substrate (Asahi VU type) was used as a sample. Grooves were fabricated by scanning of single shots, while irradiation increment was changed as an experimental parameter. By adjusting z -position of the sample, effective working distance of the optical system was investigated. Scanning electron microscopy (SEM), and confocal optical microscopy were used to evaluate the surface and shape of grooves. Also, electrical insulation of grooves was checked. All the experiments are performed under room condition. Experimental conditions are tabulated in Table 1.

3. Numerical method

In our previous study [12], temperature distribution was investigated using a thermal model considering plasma shielding, and it was found that melting depth has a critical relationship with crater depth. Therefore, influence of plasma shielding on source term of the heat equation was investigated using beam propagation method in this study. As influence of beam profile on temperature distribution during film side irradiation was of interest, only the numerical analysis in the case of film side irradiation, in which mechanism of material removal can be considered simply as vaporization and melt-ejection, was performed.

3.1. Thermal modeling considering plasma shielding

From axial symmetry of the beam, two-dimensional cylindrical coordinates were set for numerical modeling. Fig. 3 illustrates region of numerical interest. Pulsed laser ablation accompanies phase change of material such as melting and vaporization, which induce plasma shielding. The heat equation that accounts for those is written as [18–21]

$$\rho [c_p + L_m \delta(T - T_m)] \left(\frac{\partial T}{\partial t} - v_s \frac{\partial T}{\partial z} \right) = \frac{1}{r} \frac{\partial}{\partial r} \left(\kappa r \frac{\partial T}{\partial r} \right) + \frac{\partial}{\partial z} \left(\kappa \frac{\partial T}{\partial z} \right) + S \quad (1)$$

where c_p , ρ , L_m , δ , T_m , v_s , κ , and S indicate specific heat, density, latent heat of melting, the Kronecker δ -like function to define temperature range of melting, melting temperature, surface recessing velocity, thermal conductivity, and source term respectively. The term $L_m \delta(T - T_m)$ with the Kronecker δ -like function of the form

$$\delta(T - T_m, \Delta) = \frac{1}{\sqrt{2\pi}\Delta} \exp \left[-\frac{(T - T_m)^2}{2\Delta^2} \right] \quad (2)$$

allows the performance of calculation of the liquid-solid interface [18,19,21], where Δ denotes half range of phase change.

Surface recession velocity is defined assuming that the flow of vaporized material from the surface follows the Hertz-Knudsen equation, and the vapor pressure above the vaporized surface is estimated with the Clausius-Clapeyron equation [20,21].

$$v_s = (1 - \beta) \left(\frac{M}{2\pi k_B T_s} \right)^{1/2} \frac{p_0}{\rho} \exp \left[\frac{ML_v}{k_B} \left(\frac{1}{T_v} - \frac{1}{T_s} \right) \right] \quad (3)$$

Here, M , k_B , T_s , p_0 , L_v , and T_v indicate atomic mass, Boltzmann constant, surface temperature, reference pressure, latent heat of vaporization, and boiling temperature respectively. β is so called sticking coefficient which accounts for back-flux of ablated species, being approximately 0.18 [20,21].

In Eq. (1), laser heating source term S which expresses plasma shielding as well is given as.

$$S = \alpha(1 - R) \cdot I(r, z) \cdot \exp(-\alpha z) \cdot \frac{2\sqrt{\ln 2}}{t_p \sqrt{\pi}} \exp \left[-4 \ln 2 \cdot \left(\frac{t - 2t_p}{t_p} \right)^2 \right] \quad (4)$$

where α , R , I , and t_p indicate absorption coefficient, reflection coefficient between the film and ambient air, spatial intensity profile, and pulse width respectively. Considering plasma shielding, intensity profile of the beam reaches to the film surface is written as [19,20]

$$I(r, 0) = I_0 \cdot \exp(-A \cdot dZ - B \cdot E_a) \quad (5)$$

where I_0 , dZ , and E_a indicate original spatial intensity, vaporized depth, and fluence absorbed by plasma respectively. The original

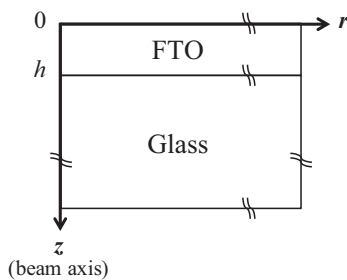


Fig. 3. Region of numerical interest.

spatial intensity profile was set as Gaussian or square of 0th-order Bessel function of the first kind. A and B are plasma absorption coefficients which is attributed to vaporized material and energy absorbed by plasma respectively. These are free parameters which can be determined based on experimental results [19,20]. Value of A and B was fitted based on the experimental results with Gaussian beam irradiation. Intensity profile inside the film was calculated by beam propagation method. The details of the method are described in the next session.

For the boundary conditions, natural convection to ambient air and radiation heat transfer can be ignored compared to heat conduction to the substrate in nanosecond regime. Hence, only the heat flux determining the surface vaporization of sample during laser pulse was taken into account [21]. Heat flux crossover z axis is 0 in cylindrical coordinates system. Interface of glass/FTO was considered as coupled boundary. Temperature boundary condition of $T = 300$ K, which is equal to initial temperature, was defined at far boundaries in axial and radial directions. Above boundary conditions are written as

$$\begin{aligned} \left. \frac{\partial T}{\partial z} \right|_{z=0} &= \rho v_s L_v, \left. \frac{\partial T}{\partial z} \right|_{r=0} = 0, \left. \kappa_{FTO} \frac{\partial T}{\partial z} \right|_{z=h} = \left. \kappa_{glass} \frac{\partial T}{\partial z} \right|_{z=h}, T(r_{max}, z) \\ &= T(r, z_{max}) = 300 \text{ K} \end{aligned} \quad (6)$$

3.2. Beam propagation during laser ablation

The free space propagation method using the Fourier transform was used to provide propagation of the electric field. Details of numerical method are well described in the articles of T. Čižmár and coworkers [15,22]. In this section, we briefly describe main features of the method focusing on the Bessel beam propagation behind the axicon. Now, the Bessel beam shaper shown in Fig. 1 is assumed as an axicon which makes plane wave refracted with semi-apex angle $\theta = 17^\circ$. When we set z -coordinate of the axicon tip as $-Z$, initial electric field is given as

$$E(r, -Z) = E_0 \exp \left(-\frac{r^2}{w_0^2} \right) \cdot \exp(-ikr \sin \theta) \quad (7)$$

where w_0 and k are original beam radius and wavenumber respectively. As the field has rotational symmetry, the 2-dimensional Fourier transform reduces to the form of the zero order Hankel transform [15]. Considering numerical treatment, the Hankel transform is a function of the form

$$S_i^{-z} = k \sum_{j=1}^N E(r_j, -Z) r_j \Delta r_j J_0(k \mathcal{R}_j r_i) \quad (8)$$

$$S_i^z = S_i^{-z} \exp \left(ikz \sqrt{1 - \mathcal{R}_i^2} \right) \quad (9)$$

where $\Delta r_j = r_{j+1} - r_j$ is the length of the j -th step in the radial direction, and \mathcal{R} denotes the normalized wavevector projection onto the r coordinate ($\mathcal{R} = r/r_{max}$). Superscript and subscript of S indicate z -coordinate and step index in the radial direction respectively. The electric field is obtained by inverse Hankel transform of Eq. (9).

$$E_i^z = k \sum_{j=1}^N \mathcal{R}_j \Delta \mathcal{R}_j S_j^z J_0(k \mathcal{R}_j r_i) \quad (10)$$

where $\Delta \mathcal{R}_j = \mathcal{R}_{j+1} - \mathcal{R}_j$. Square root of attenuation factor $\exp[(-A \cdot dZ(r) - B \cdot E_a(r))/2]$ in Eq. (5) is multiplied in Eq. (10) at the film surface $z = 0$. Consequently, intensity field is given from correlation

$$I = \frac{cn_0}{2} E^2 \quad (11)$$

Table 2
Physical properties of materials.

Parameter	Unit	SnO ₂ [23,24] (Temperature (K))	Glass [25]
Density	kg/m ³	6950	2520
Specific heat, c_p	J/(kg·K)	$3520 \times 10^{-4} \cdot T + 200$ $7750 \times 10^{-5} \cdot T + 475$ 614	837
Latent heat of melting, L_m	J/kg	3.17×10^5	–
Melting temperature, T_m	K	1898	722 (softening)
Latent heat of vaporization, L_v	J/kg	2.08×10^6	–
Boiling temperature, T_b	K	2273	–
Thermal conductivity, κ	W/(m·K)	30 $4540/T^{0.88}$ 5	1
Absorption coefficient, α	m ⁻¹	1.5×10^5	–
A	m ⁻¹	1.5×10^6	–
B	m ² /J	9.6×10^{-4}	–
Half range of phase change, Δ	K	50	–
Film thickness, h	nm	650	–
Refractive index, n	–	1.6 [4] at 1064 nm	1.51 at 1064 nm
Atomic mass, M	g/mol	150.71	–

where c , n , and ϵ_0 are speed of light in vacuum, refractive index, and permittivity of vacuum respectively. Substituting Eq. (11) into Eq. (4), intensity distribution affected by plasma shielding is obtained so as to provide source term in heat equation.

In this study, implicit numerical scheme of finite differential method was implemented for heat equation, and source term by means of beam propagation method was explicitly renewed in every time step. Physical properties of materials are tabulated in Table 2. Temperature dependence of several properties was considered [23,24].

4. Results and discussion

4.1. Scribing quality

Grooves are fabricated by successive irradiation of single shot with constant pitch. Fig. 4 shows SEM images of grooves fabricated by Bessel beam with substrate side irradiation at fluence of 9.0 J/cm², 12.0 J/cm², and 15.0 J/cm². Irradiation pitch were 0.5 μ m, 1.0 μ m, and 1.0 μ m respectively. Averaged width of the grooves were 2.3 μ m, 3.3 μ m, and 3.0 μ m respectively. It is significantly narrow compared to the cases of several-tens-micrometers-wide Gaussian beam scribing. Electrical isolation was confirmed for the represented cases. However, electrically isolated groove could not be scribed with the pitch of 1.0 μ m in the case of 9.0 J/cm². Narrower width of groove was achieved by fluence of 9.0 J/cm² while fabrication speed decreased by small irradiation pitch. Obviously, depth and width of crater fabricated by single shot has significant effect on fabrication speed which is determined by irradiation pitch.

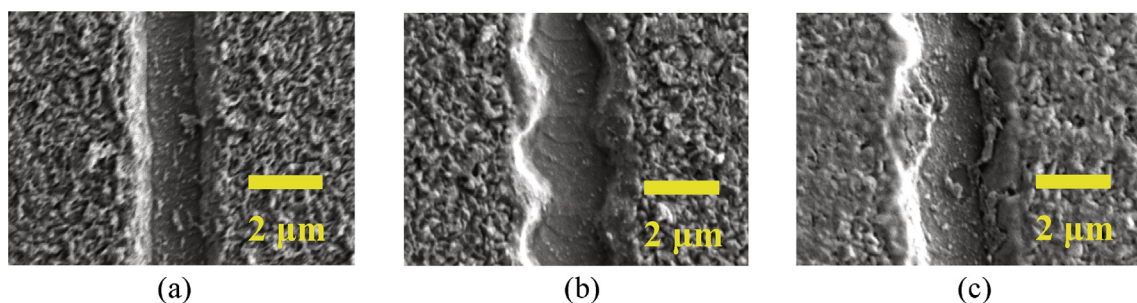


Fig. 4. SEM images of groove fabricated by Bessel beam with substrate side irradiation. (a) 9.0 J/cm², (b) 12.0 J/cm², (c) 15.0 J/cm². Considerably narrow scribing with 2.3–3.3 μ m width was achieved.

As fluence increases, step structure affected by heating of intense side lobe of Bessel beam appears remarkably. For thermal ablation, the heating by side lobes of Bessel beam inevitably results in processing defects. This is critical disadvantage of Bessel beam process compared to Gaussian beam process. As an effort to suppress side lobe intensity, S. Mori suggested an optical manipulation using interference of two annular beams [26].

4.2. Sample positioning robustness in axial direction

As indicated in Fig. 2, the Bessel beam generated in this study had considerably deep focal depth of 11.5 mm. In order to investigate robustness of sample positioning in axial direction, we changed z -position of the sample for the irradiation conditions indicated in Fig. 4. Fig. 5 shows mapping of electrical isolation with respect to z position of the sample. Electrically isolated grooves have been obtained in the range of 6–11 mm of axial direction. Generally, Gaussian beam focused by convex lens or object lens has focal depth of several tens micrometers to sub millimeters depending on focal depth. As Gaussian beam gets focused narrower, processible range decreases significantly with decreasing focal depth. On the other hand, considerably large processible range of the Bessel beam can ensure stable operation with critically narrow beam width beyond diffraction limit.

4.3. Effect of irradiation direction compared to Gaussian beam

Regardless of irradiation direction, the film surface temperature increases most so that plasma shielding during nanosecond laser pulse becomes prominent at the film surface. Therefore, ablation

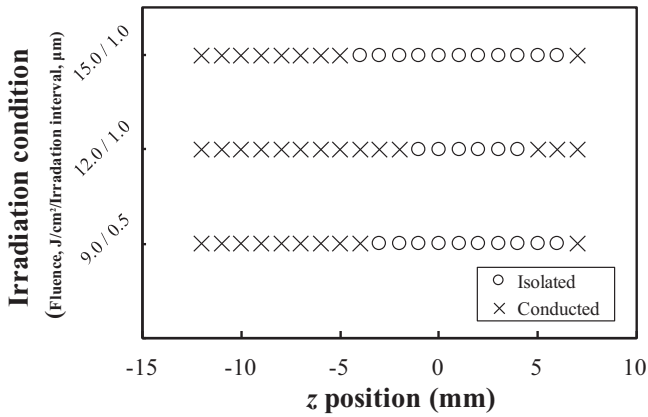


Fig. 5. Mapping of electrical isolation with respect to z position of the sample. Fluence/irradiation pitch of the indicated cases is $9.0\text{ J/cm}^2/0.5\ \mu\text{m}$, $12.0\text{ J/cm}^2/1.0\ \mu\text{m}$, and $15.0\text{ J/cm}^2/1.0\ \mu\text{m}$ respectively. Electrical isolation was confirmed in 6–11 mm range of axial direction.

depth of film side irradiation by single shot is limited even though fluence is increased considerably. Fig. 6 indicates crater depth fabricated by single shot irradiation of Gaussian beam and Bessel beam with both film side and substrate side irradiation. Calculation results of melting depth at $t = t_p$, when most of the laser beam is absorbed, are depicted as well. Shade area of diagonal pattern indicates region that film/substrate interface may exist according to the sample specification. From the fact that area near boundary of the grooves in Fig. 4 keeps sample’s original texturized structure [27], it is supposed that most of melting material was removed by evaporation or melt-ejection which is induced by expansion of plasma accompanying shockwave. Thus, experimentally measured depth of the craters is compared with calculated melting depth in this study. Irrespective to beam profile, film was drilled completely by substrate side irradiation from the fluence greater than 10.6 J/cm^2 , because the plasma shielding had almost no effect on the beam absorption. However, dependence on the beam profile is seen remarkable in the case of film side irradiation. The FTO film was drilled no more than 530 nm with film side irradiation of Gaussian beam, even with significantly large fluence of 354 J/cm^2 . On the other hand, the film was completely removed by single shot irradiation of the Bessel beam at fluence greater than 16.0 J/cm^2 . Calculated melting depth reaches to the film thickness from

the fluence greater than 16.0 J/cm^2 as well. Although the plasma absorption parameters A and B in Eq. (5) were fitted with experimental results of the Gaussian beam irradiation, the calculation results showed good agreement with experimental results of the Bessel beam irradiation as well. As ablation of substrate material was not considered in the numerical model, maximum melting depth is equal to the film thickness. The model is not accounting for strict mechanism of melt ejection and formation of crater. Thus, deviation between experimental results exists especially at small fluences when melt ejection induced by plume expansion may not be prominent.

From the fact that the model predicted the experimental results with acceptable deviation, self-reconstruction of the Bessel beam can be considered as a critical factor which contributes to single shot removal with film side irradiation. Fig. 7 represents the calculated axial intensity of the beam inside the film at the peak of the pulse, $t = 0$. With increasing fluence, axial intensity of the Gaussian beam decreased drastically because of plasma shielding at the surface. However, axial intensity of the Bessel beam was reconstructed inside the film resulting in continuous heating.

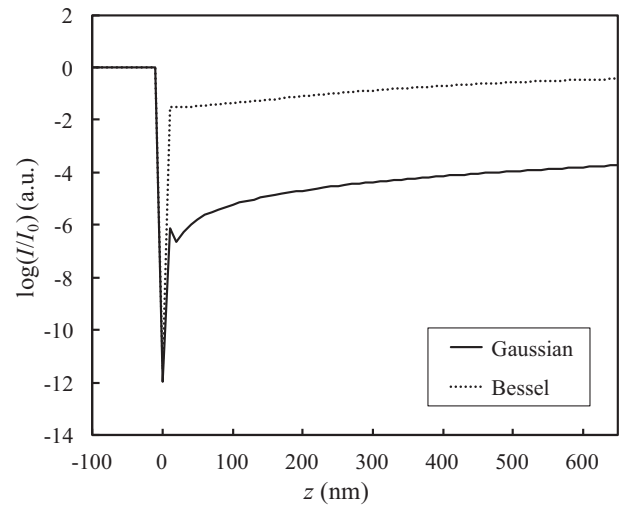


Fig. 7. Axial intensity of Gaussian beam and Bessel beam inside the film with fluence of 16.0 J/cm^2 at $t = 0$. Intensity of the Bessel beam is reconstructed behind the film surface while that of the Gaussian beam decreased critically.

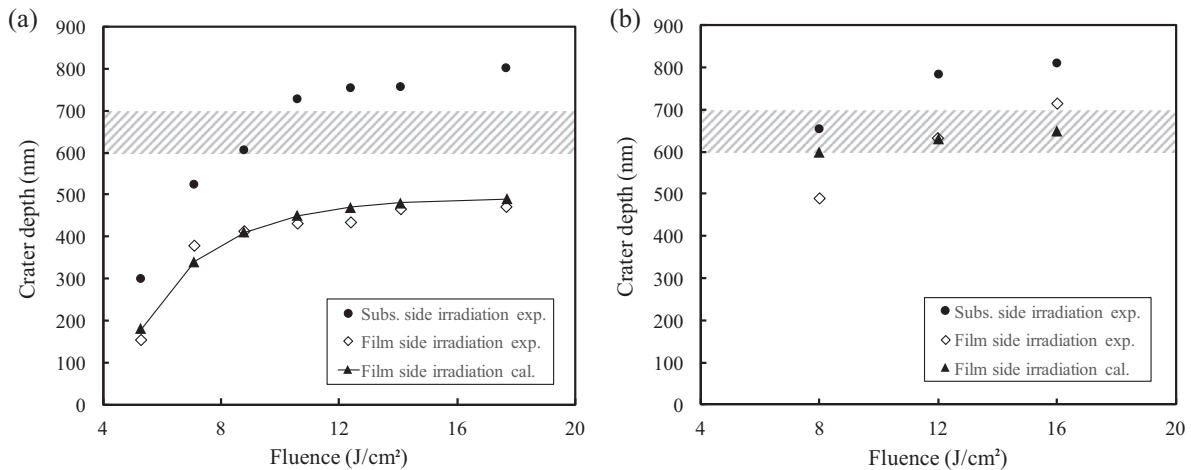


Fig. 6. Crater depth obtained by single shot irradiation and calculated melting depth. (a) Gaussian beam irradiation, (b) Bessel beam irradiation. Film side irradiation of Bessel beam leads to complete removal of the film by single shot. The numerical model in which plasma shielding and beam propagation are coupled well predicted crater depth in terms of melting depth.

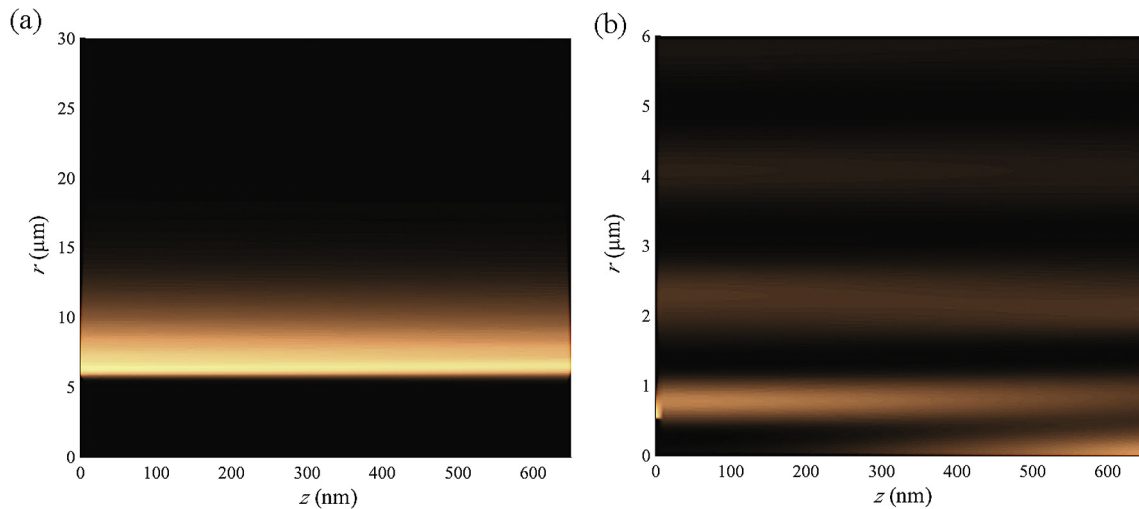


Fig. 8. Intensity distribution of (a) Gaussian beam and (b) Bessel beam inside the film with fluence of 16.0 J/cm^2 at $t = 0$. Significant intensity was obtained by self-reconstruction followed by diffraction of the Bessel beam (right bottom of the (b)) becomes significant just behind the obstacle of which size is smaller than area of 0th order lobe.

Fig. 8 illustrates two-dimensional intensity distribution of the Gaussian beam and Bessel beam with fluence of 16.0 J/cm^2 at $t = 0$. Each color map was normalized by maximum intensity before plasma shielding. Usually, Bessel beam generated by axicon has significantly large semi apex angle compared to Gaussian beam focused by convex lens, unless object lens with critically large NA is used for focusing. Thus, Bessel beam has relatively strong self-reconstruction at short distance behind the obstacle. Furthermore, critical intensity just behind the plasma shielding can be easily obtained by self-reconstruction followed by diffraction, which is attributed to significantly small area of plasma shielding formed by Bessel beam. It is well represented at the right bottom side of Fig. 8(b).

Laser scribing with substrate side irradiation is difficult to be applied industrially because the surface of thin film contacts the working stage. This undesirable contact may be prevented by supporting only the edges of the substrate. However, substrate with low rigidity such as polymer material cannot be supported by this method. Furthermore, use of substrate side irradiation is strongly dependent on absorption spectra of the substrate material. We would like to emphasize that Bessel beam can be used as a versatile tool for scribing of the thin film with sub-micrometer thickness with wide selectivity of substrate material by improving processing quality and minimizing effect of plasma shielding.

5. Conclusion

The general features of Bessel beam scribing of the TCO thin film with 600–700 nm thickness were given and compared with Gaussian beam scribing. As a result, significantly narrow P1 scribing of 2.3–3.3 μm width was achieved with electrical isolation. It is worthy to emphasize that the significantly narrow P1 groove which was fabricated by our Bessel beam is comparable with the groove fabricated by fs laser. In our best knowledge, it is the first time that a groove with width of 2.3–3.3 μm was fabricated by ns laser. In addition, due to considerably deep focal depth, electrically isolated grooves were scribed when the sample was set in the range of 6–11 mm in the optical direction. We also investigated characteristics of film side irradiation using numerical method in which plasma shielding and beam propagation are coupled. The calculation results showed great agreement with experimental

results obtained by single shot irradiation. Beam propagation method which accounts for self-reconstruction of Bessel beam well explained the single shot removal mechanism of film side irradiation. We expect that ns laser scribing system of thin film with sub-micron thickness can be implemented efficiently by using Bessel beam without selecting substrate material.

Acknowledgements

Part of this work has been supported by JSPS KAKENHI Grant Number 15J10556 and Amada Foundation, Japan. B. Kim represents special gratitude to JSPS.

References

- [1] J. Bovatsek, A. Tamhankar, R.S. Patel, N.M. Bulgakova, J. Bonse, *Thin Solid Films* 518 (2010) 2897–2904.
- [2] D. Canteli, S. Fernandez, C. Molpeceres, I. Torres, J.J. Gandía, *Appl. Surf. Sci.* 258 (2012) 9447–9451.
- [3] D. Canteli, I. Torres, J.J. García-Ballesteros, J. Càrabe, C. Molpeceres, J.J. Gandía, *Appl. Surf. Sci.* 271 (2013) 223–227.
- [4] H. Wang, S.T. Hsu, H. Tan, Y.L. Yao, H. Chen, M.N. Azer, *J. Manuf. Sci. Eng.* 135 (2013) 051004.
- [5] S.F. Tseng, W.T. Hsiao, D. Chiang, C.K. Chung, J.L.A. Yeh, *Opt. Lasers Eng.* 52 (2014) 212–217.
- [6] S. Krause, P.-T. Miclea, F. Steudel, S. Schweizer, G. Seifert, *J. Renewable Sustainable Energy* 6 (2014) 011402.
- [7] D.H. Doan, R. Iida, B. Kim, I. Satoh, K. Fushinobu, *J. Therm. Sci. Technol. JPN* 11 (2016) 1.
- [8] N. Iwatani, H.D. Doan, K. Fushinobu, *Int. J. Heat Mass Transfer* 71 (2014) 515–520.
- [9] B. Kim, R. Inoue, H.D. Doan, K. Fushinobu, *Trans. Jpn. Soc. Mech. Eng.* 80 (815) (2014) (in Japanese).
- [10] Y.P. Meshcheryakov, N.M. Bulgakova, *Appl. Phys. A* 82 (2006) 363–368.
- [11] Y.P. Meshcheryakov, M.V. Shugayev, T. Mattle, T. Lippert, N.M. Bulgakova, *Appl. Phys. A* 113 (2013) 521–529.
- [12] B. Kim, R. Iida, H.D. Doan, K. Fushinobu, *Int. J. Heat Mass Transfer* 102 (2016) 77–85.
- [13] A.E. Hussein, P.K. Diwakar, S.S. Harilal, A. Hassanein, *J. Appl. Phys.* 113 (2013) 143305.
- [14] Z. Bouchal, J. Wagner, M. Chlup, *Opt. Commun.* 151 (1998) 207–211.
- [15] O. Brzobohatý, T. Čížmár, P. Zemánek, *Opt. Express* 16 (17) (2008) 12688.
- [16] V. Karásek, O. Brzobohatý, P. Zemánek, *J. Opt. A: Pure Appl. Opt.* 11 (2009) 034009.
- [17] X. Tsampoula, V. Garcés-Chávez, D.J. Stevenson, B. Agate, C.T.A. Brown, F. Gunn-Moore, K. Dholakia, *Appl. Phys. Lett.* 91 (2007) 053902.
- [18] S.P. Zhvayvi, G.D. Ivlev, *J. Eng. Phys. Thermophys.* 69 (1996) 608–611.
- [19] N.M. Bulgakova, A.V. Bulgakov, L.P. Babich, *Appl. Phys. A* 79 (2004) 1323–1326.
- [20] N.M. Bulgakova, A.V. Bulgakov, *Appl. Phys. A* 73 (2001) 199–208.

- [21] M. Stafe, A. Marcu, N. Puscas, *Pulsed Laser Ablation of Solids Basics, Theory and Applications*, Springer, 2013.
- [22] T. Čížmár, (Ph.D. thesis), Masaryk University in Brno, 2006.
- [23] G.V. Samsonov, *The Oxide Handbook*, IFI/Plenum, 1982.
- [24] A. Berthelot, F. Gourbilleau, C. Dufour, B. Domengès, E. Paumier, *Nucl. Instr. Meth. Phys. Res. B* 166–167 (2000) 927–932.
- [25] The Japan Society of Mechanical Engineers ed., “JSPS Data Book Heat Transfer”, The Japan Society of Mechanical Engineers (in Japanese), 1986. p. 320.
- [26] S. Mori, *Precis. Eng.* 39 (2015) 79–85.
- [27] M. Kambe, N. Taneda, A. Takahashi, T. Oyama, *Res. Reports Asahi Glass Co. Ltd.* 60 (2010) (in Japanese).